Metal and Semiconductor Nanowire Network Thin Films with Hierarchical Pore Structures

Donghai Wang,[†] Hans Peter Jakobson,[‡] Rong Kou,[†] Jing Tang,[†] Robert Z. Fineman,[†] Donghong Yu,[‡] and Yunfeng Lu*,[†]

Department of Chemical & Biomolecular Engineering, Tulane University, New Orleans, Louisiana 70118 and Department of Life Sciences, Section for Chemistry, Aalborg University, 9000 Aalborg, Denmark

Received October 5, 2005. Revised Manuscript Received June 3, 2006

Metal and semiconductor nanowire thin films with hierarchical pore structure were electrodeposited using mesoporous silica (primary porogens) containing colloidal silica particles (secondary porogens) as templates. The pore size of the nanowire thin films was independently controlled by the wall thickness of the surfactant-templated mesopores and the sizes of the incorporated silica particles. The mesostructure of the nanowire thin films (e.g., hexagonal and cubic mesostructures) was controlled by judicious choice of surfactant. Furthermore, the shape of the secondary pores (e.g., sphere and rod shapes) can be controlled using secondary porogens with various shapes. Such hierarchical nanowire thin films provide novel platforms for photovoltaic, sensor, and other device applications. To demonstrate the advantage of such hierarchical porous networks, we fabricated photovoltaic devices by infiltrating the hole-conducting poly-(3-hexylthiophene) into the electron-conducting CdSe nanowire thin films with and without the secondary pore channels. The heterojunction solar cells consisting of a CdSe nanowire network with secondary pore structure and poly(3-hexylthiophene) showed improved performance with a short-circuit current of 2.4 mA/cm^2 under AM 1.5 solar illumination, confirming the advantages of such hierarchical pore structure for actual device applications.

Introduction

Materials with nanoscale structure, such as quantum dots, nanocrystals, nanorods, nanowires, nanotubes, and nanomeshes, often show novel electronic, magnetic, optical, thermal, or mechanical properties, holding great promise for a wide spectrum of applications.[1] However, realization of these promises requires translation of the nanoscale components into micro/macroscale dimensions that are required for device applications. One of the most significant efforts toward this goal is direct synthesis or assembly of nanoscale components into macroscopic architectures such as arrays,[2,3] networks,[4,5] or more complicated hierarchical structures.[6]

To date, nanowire networks can be prepared through either a templateless[7−9] or a templating approach.[5] For example, Au and Se nanowire networks have been prepared by coalescing Au nanoparticles or preferential crystal facet growth of Se microspheres.[7,8] Biomimetic approaches have also been used to synthesize wire networks with hierarchically organized morphologies.[10] However, the templateless synthesis often lacks control over the nanowire dimension, pore structure, and chemical compositions. We recently developed a simple and generalized approach toward the synthesis of supported nanowire network thin films by combining electrodeposition and mesoporous silica templating techniques.[11,12] Currently the pore dimension of such nanowire networks is determined by the wall thickness of the silica framework, which is often limited to 2−3 nm according to the available templates. Such uniform but

* To whom correspondence should be addressed. E-mail: ylu@tulane.edu.
† Tulane University.
‡ Aalborg University.

(1) Xia, Y.; Yang, P.; Sun, Y.; Wu, Y.; Mayers, B.; Gates, B.; Yin, Y.; Kim, F.; Yan, H. One-dimensional nanostructures: Synthesis, characterization, and applications. *Adv. Mater.* **2003**, *15* (5), 353−389.
(2) Huang, M. H.; Mao, S.; Feick, H.; Yan, H.; Wu, Y.; Kind, H.; Weber, E.; Russo, R.; Yang, P. Room-temperature ultraviolet nanowire nanolasers. *Science* **2001**, *292* (5523), 1897−1899.
(3) Lopes, W. A.; Jaeger, H. M. Hierarchical self-assembly of metal nanostructures on diblock copolymer scaffolds. *Nature* **2001**, *414* (6865), 735−8.
(4) Ryan, K. M.; Erts, D.; Olin, H.; Morris, M. A.; Holmes, J. D. Three-Dimensional Architectures of Ultra-high-Density Semiconducting Nanowires Deposited on Chip. *J. Am. Chem. Soc.* **2003**, *125* (20), 6284−6288.
(5) Shin, H. J.; Ryoo, R.; Liu, Z.; Terasaki, O. Template Synthesis of Asymmetrically Mesostructured Platinum Networks. *J. Am. Chem. Soc.* **2001**, *123* (6), 1246−1247.
(6) Tian, Z. R.; Voigt, J. A.; Liu, J.; McKenzie, B.; McDermott, M. J.; Rodriguez, M. A.; Konishi, H.; Xu, H. Complex and oriented ZnO nanostructures. *Nat. Mater.* **2003**, *2* (12), 821−826.
(7) Ramanath, G.; D′Arcy-Gall, J.; Maddanimath, T.; Ellis, A. V.; Ganesan, P. G.; Goswami, R.; Kumar, A.; Vijayamohanan, K. Templateless Room-Temperature Assembly of Nanowire Networks from Nanoparticles. *Langmuir* **2004**, *20* (13), 5583−5587.
(8) Cao, X.; Xie, Y.; Li, L. Spontaneous organization of three-dimensionally packed trigonal selenium microspheres into large-area nanowire networks. *Adv. Mater.* **2003**, *15* (22), 1914−1918.
(9) Walsh, D.; Arcelli, L.; Ikoma, T.; Tanaka, J.; Mann, S. Dextran templating for the synthesis of metallic and metal oxide sponges. *Nat. Mater.* **2003**, *2* (6), 386-390.
(10) Yu, S.-H.; Antonietti, M.; Coelfen, H.; Hartmann, J. Growth and Self-Assembly of BaCrO4 and BaSO4 Nanofibers toward Hierarchical and Repetitive Superstructures by Polymer-Controlled Mineralization Reactions. *Nano Lett.* **2003**, *3* (3), 379−382.
(11) Wang, D.; Luo, H.; Kou, R.; Gil Maria, P.; Xiao, S.; Golub Vladimir, O.; Yang, Z.; Brinker, C. J.; Lu, Y. A general route to macroscopic hierarchical 3-D nanowire networks. *Angew. Chem., Int. Ed.* **2004**, *43* (45), 6169−73.

10.1021/cm052216b CCC: $33.50
Published on Web 08/03/2006

Scheme 1. Schematic Illustration of Fabrication of a Nanowire Network Thin Film with Hierarchically Controllable Pore Structure[a]

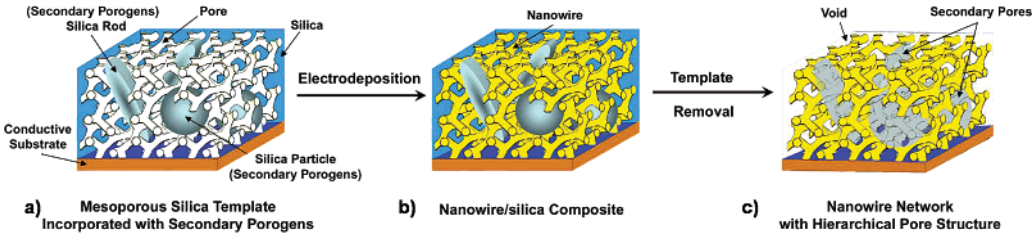

[a] (a) Formation of a mesoporous silica thin film template containing secondary porogens on a conductive substrate by evaporation-induced self-assembly (EISA) of silicates, surfactant, and silica particles followed by surfactant removal. (b) Electrochemical growth of metal or semiconductors within the template resulting in a metal or semiconductor nanowire/silica nanocomposite thin film. (c) Removal of silica, including primary and secondary porogens, leads to a nanowire network thin film with controllable hierarchical pore structure.

relatively small pores may limit the efficiency of mass transport across the networks,[13] although this approach still represents a highly flexible way to synthesize nanowire networks in terms of chemical composition, internal structure, thermal stability, and precise control over the nanowire diameter.

We present here a generalized approach to fabricate continuous nanowire network films with controllable pore structure at the meso- and macroscale. The introduction of macropores in addition to the mesopores is achieved by incorporating silica particles to the original mesoporous template. As depicted in Scheme 1, a supported silica thin film template is synthesized with coexistence of mesoporous silica that is formed by co-assembly of surfactant and silicate clusters (denoted as primary porogens) and colloidal silica particles (denoted as secondary porogens). Silica particles in various shapes (e.g., rod or spherical) can be used as the secondary porogens. Electrodeposition continually grows metal or semiconductor materials within the mesoporous channels from the bottom of the film upward until the mesoporous channels are completely filled. The simultaneous removal of the primary and secondary templates creates nanowire networks with pore structures hierarchically controlled at both meso- and macroscales. The diameters (e.g., 2−20 nm) of the nanowires are controlled by the diameter of mesopores, and mesostructure of the nanowire thin films is readily controlled from two-dimensional hexagonal (2-D wire-like) to three-dimensional cubic (3-D mesh-like) structure. One distinguished feature of this approach is that the pore sizes across different length scales are independently controlled by the sizes of the primary and secondary porogens. Since the secondary porogens are commercially available in various sizes (e.g., 20−300 nm) and shapes (e.g., spherical, rod-shaped), this strategy provides a significant scope to construct the hierarchical pore structure in the nanowire networks. Creating such hierarchical pores within the continuous nanowire networks allows more efficient mass transport through the thin films and facilitates infiltration of guest components (e.g., hole-conducting molecules) into a porous nanowire network, providing novel nanostructured platforms for device applications, such as photovoltaics, sensors, and electrodes.

Experimental Section

Materials. Tetraethyl orthosilicate (TEOS, $Si(OC_2H_5)_4$, 98%), ethanol(200 proof), hydrochloric acid (HCl, 37.5%), sodium hydroxide (NaOH), nonionic surfactant Brij-58 ($C_{16}H_{33}(OCH_2CH_2)_{20}OH$), nonionic surfactant Brij-56 ($C_{16}H_{33}(OCH_2CH_2)_{10}OH$), cadmium sulfate ($CdSO_4$, 98%), selenium dioxide (SeO_2, 99.99%), hexachloroplatinic acid aqueous solution (10% H_2PtCl_6), and ethanolamine ($H_2NCH_2CH_2OH$, 98%) were purchased from Aldrich. Triblock copolymer Pluronic P123 ($EO_{20}PO_{70}EO_{20}$, EO and PO are used to designate ethylene oxide and propylene oxide, respectively) was donated by BASF. Spherical colloidal silica (SNOWTEX-20L, 20%, diameter 40−50 nm), spherical colloidal silica aqueous solution (SNOWTEX-ZL, 40%, diameter 70−100 nm), and elongated colloidal silica aqueous solution (SNOWTEX-OUP, 15%, diameter of 9−15 nm with length of 40−300 nm) were donated from Nissan Chemicals. The above chemicals were used without further purification. Indium-doped tin oxide (ITO) glass slides were purchased from Delta Technologies. Fluorine-doped tin oxide (FTO) glass slides were purchased from Pilkington. ITO and FTO glass slides were cleaned by soaking in 20% ethanolamine aqueous solution at 70 °C for 1 h. Poly(3-hexylthiophene) was purchased from Aldrich and purified as follows: 0.035 g of P3HT was dissolved in 25 mL of $CHCl_3$ and then filtered to get a dark yellow solution. After adding 20−30 mL of methanol, purple precipitates formed and were collected by filtration. The resulting polymer was put into a vacuum oven at room temperature overnight.

Synthesis of Mesoporous Silica Films. Mesoporous silica thin films were deposited on ITO (for Pt electrodeposition) or FTO (for CdSe electrodeposition) glass slides by dip coating at 7 cm/min in precursor solutions of silicate/surfactant/silica particle followed by calcinations. P123 was used as a structural agent to direct 2-D hexagonal pore structure of the mesoporous silica templates. A typical sol is prepared by dissolving 1 mL of TEOS, 0.25 g of P123, or 0.25 g of Brij56 using 4.2 g of ethanol in a vial followed by addition of 0.4 g of 0.1 N HCl aqueous solutions and sonicating for 30 min to 1 h at room temperature to allow for hydrolysis and condensation of the TEOS. Brij-58 and Brij-56 were used as the pore structure directing agent to synthesize 3-D cubic mesoporous templates with an average mesopore diameter of 5 nm. A typical sol is prepared by dissolving 1 mL of TEOS and 0.3 g of Brij-58 (0.25 g of Brij-56) in 4.2 g of ethanol followed by addition of 0.4 g of 0.3 N HCl (0.1 N HCl) aqueous solutions in a vial and sonicating for 2 h at room temperature.

(12) Wang, D.; Zhou, W. L.; McCaughy, B. F.; Hampsey, J. E.; Ji, X.; Jiang, Y.-B.; Xu, H.; Tang, J.; Schmehl, R. H.; O'Connor, C.; Brinker, C. J.; Lu, Y. Electrodeposition of metallic nanowire thin films using mesoporous silica templates. *Adv. Mater.* **2003**, *15* (2), 130−133.
(13) Wang, D.; Kou, R.; Gil Maria, P.; Jacobson, H. P.; Tang, J.; Yu, D.; Lu, Y. The templated synthesis, characterization and sensing application of macroscopic Pt nanowire network electrodes. *J. Nanosci. Nanotechnol.* **2005**, *5*(11), 1904−1909.

The precursor solution for mesoporous silica template containing secondary porogens was prepared as follows: 0.5 g of Pluronic P123, 0.6 g of Brij58, or 0.5 g of Brij56 was dissolved in 1.5 g of ethanol followed by addition of 1.836 g of TEOS under stirring. Then 0.5 g of a solution (adjusted to pH 1 using concentrated HCl) of colloidal silica was dropwise added to the prepared solution under vigorous stirring at room temperature. In the case of using colloidal silica porogens SNOWTEX-OUP with increased amount, 2 g of a solution of the colloidal silica (pH 1) was also dropwise added to the prepared silicate cluster/surfactant solution (i.e., 5 wt % colloidal silica in precursor solution) to investigate concentration effects on morphology. After adding the colloidal silica solution, the solution was vigorous stirred for 1 (P123) or 2 h (Brij 58 and Brij 56). Dip coating conductive glass slides into the precursor sols resulted in silica colloidal particle-doped mesostructured silica films. As-synthesized films were aged at room temperature for 4 h followed by calcinations in air for 1 h at 400 °C (heating rate, 1 °C/min). Before use of colloidal silica solutions, the pH of the colloidal solution was adjusted to 1 using 37 wt % HCl. Spherical colloidal silica solution (SNOWTEX-ZL) was diluted 6 times by adding ethanol followed by adjusting the pH to 1 using 37 wt % HCl.

Electrodeposition. The electrodeposition process was conducted in a conventional three-electrode cell using a saturated calomel reference electrode (SCE), a Pt wire counter electrode, and mesoporous silica-coated conductive glass slides as the working electrode. Pt electrodeposition was conducted in 2 wt % H_2PtCl_6 precursor solutions using a galvanostatic pulse current (a periodic galvanostatic pulse train of 100 ms of 0.5 mA/cm^2 and 2 s at 0 mA/cm^2) for 30 min to deposit Pt nanowire films around 200 nm thick. The nanowire network was obtained after removing the silica template using 1% HF solution for 5 min operated in fume hoods (use of HF solution should follow the manufacturers' recommended safety procedures). Etching a short time (e.g., 30 s) partially preserves the silica colloids.

CdSe nanowire network thin films were electrodeposited on mesoporous silica-coated FTO electrode for following photovoltaic device fabrication. CdSe electrodeposition was conducted in a plating solution of CdSe containing 0.2 M $CdSO_4$, 1.0 mM SeO_2 adjusted with HCl to pH 2.5. The CdSe was deposited potentiostatically at −0.650 V vs SCE at 85 °C. As-deposited CdSe/silica composite films were annealed at 600 °C in Ar for 20 min. The nanowire network was obtained after soaking in 2 M NaOH solution at 70 °C overnight.

Fabrication of Photovoltaic Devices. Photovoltaic cells of FTO/CdSe nanowire network/poly(3-hexylthiophene) (P3HT)/Au were fabricated as follows. CdSe nanowire networks were prepared using Brij-56-directed cubic-structured mesoporous silica as a template. Porous-structured CdSe nanowire networks were prepared using the template with incorporating rod-shaped silica particles (SNOWTEX-OUP). A 100 nm thick CdSe nanowire network was deposited onto glass substrates coated with fluorine-doped tin oxide (FTO). A 10 mg/mL chloroform solution of P3HT was spin cast onto the CdSe nanowire network. The polymer films were typically of a thickness between 100 and 150 nm. The samples were subsequently annealed in Ar at 200 °C for 3 min and cooled to room temperature in Ar, followed by thermal evaporation of a 100 nm thick Au electrode. To prevent electrons in CdSe from reaching the Au top electrode, a second layer of polymer was spin-casted and annealed onto the porous CdSe nanowire network followed by evaporation of the Au electrode.

Characterization. The nanowire networks were investigated using X-ray diffraction (Siemen D5000, Cu Kα radiation), transmission electron microscopy (TEM, JEOL 2011 FasTEM electron microscope at 180 kV), and scanning electron microscopy (SEM, LEO 1550 VP at 10 kV). TEM samples were scratching off the substrate and put on copper grids. SEM samples were mounted on a sample holder and characterized in a top-view manner. XRD patterns of CdSe nanowire network thin films were performed using 2θ scan with a fixed incident angle at 1°. $I-V$ curve measurements of photovoltaic devices were carried out using Solartron 1287 under illumination of 100 mW/cm^2 Solar Simulator (PV Measurements, Inc. at 12.0 V corresponding to AM1.5 Global Reference Spectrum)

Results and Discussion

1. Hierarchically Porous 2-D Nanowire Thin Films. Figure 1 shows SEM images of porous Pt nanowire network thin films produced using mesoporous silica containing 2-D hexagonal pore channels with/without incorporation of secondary porogens. Similar to our previous reports,[12] the Pt nanowire film (Figure 1a) prepared using only a 2-D hexagonal template possesses swirling high-density nanowires resulting from the swirling mesoporous channels in the template. Introduction of spherical colloidal silica particles (40−50 nm in diameter) into the template results in formation of nanowires with a more dense swirling structure (see Figure 1b). The inset in Figure 1b shows a secondary pore surrounded by swirling nanowires, which indicates that the tubular silicate/surfactant mesophase may prefer to co-assemble tangential to the surface of the added silica particles, resulting in generated nanowires swirling along the secondary porogens. Incorporation of colloidal silica in the 2-D hexagonal-structured silicate/surfactant mesophase may also promote greater defect structure, resulting in more swirling structures in the 2-D nanowire networks. Figure 1c shows a hierarchically porous nanowire network produced by incorporation of spherical colloidal silica particles (70−100 nm in diameter) within the template. The existence of large pores in the range of 70−100 nm as indicated by the arrow manifest the efficiency of the secondary porogens. Randomly intertwined nanowires swirl tangentially, passing along/around the macropores, showing a significantly different morphology compared with previous dense nanowires (Figure 1a). The average nanowire diameter in porous nanowire networks is approximately 9 nm, which agrees well with the diameter of hexagonal mesopores prepared using P123. Figure 1d shows an SEM image of a Pt nanowire/silica composite thin film after partial removal of the spherical silica colloids by etching a shorter time (see Experimental Section). Spherical silica particles are heterogeneously encapsulated within mesoporous silica or nanowire networks, indicating randomly dispersed spherical secondary pores within nanowire networks after complete removal of silica template. The inset SEM image in Figure 1d shows a spherical silica particle surrounded by swirling nanowires, further confirming that hexagonal mesopores tangentially assemble along/around the added silica porogens.

The morphological shape of the secondary pore within porous nanowire networks can be varied by choosing different shapes of colloidal silica particle. Figure 1e shows a high-magnification SEM image of a Pt nanowire/silica composite thin film prepared with addition of commercial rod-shaped silica particles after partial removal of templates. Irregular-shaped silica rods residual (marked by a yellow arrow) and rod-shaped secondary pores (marked by a white

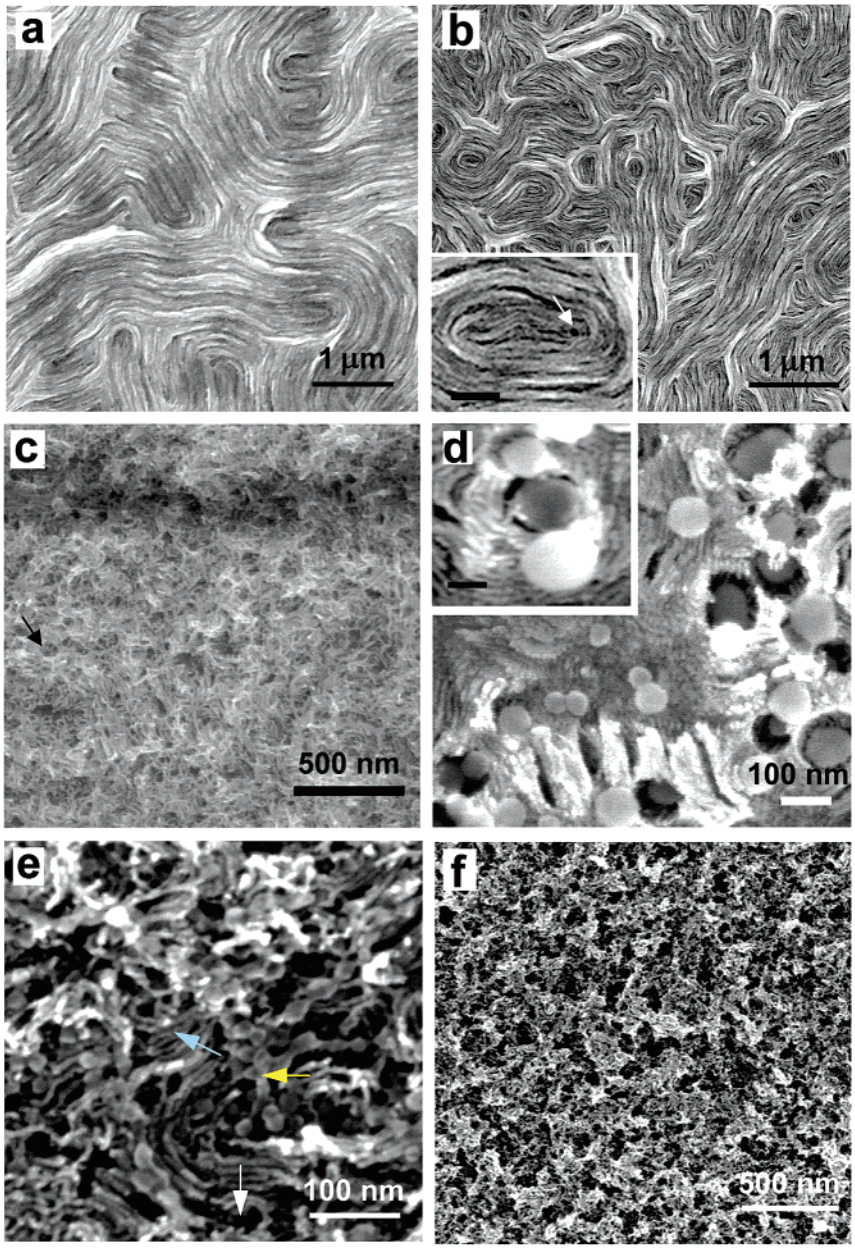

Figure 1. SEM images of porous Pt nanowire networks prepared using P123-directed tubular structured mesoporous silica templates containing different secondary porogens. (a) Pt nanowire thin film without incorporating secondary pores. (b) Pt swirling nanowire thin film prepared using templates containing 40 nm spherical silica particles as secondary porogens. (Inset) High-magnification SEM image of the sample. A spherical secondary pore is marked by an arrow. Scale bar in the inset is 200 nm. (c) Highly porous Pt nanowire network prepared using templates containing 70−100 nm spherical silica particles as secondary porogens. A spherical secondary pore is marked by an arrow. (d) Pt nanowire/silica composite after partial silica removal showing spherical silica particles embedded in the nanowire/silica composite. (Inset) High-magnification SEM image. Pt nanowires partially swirl around spherical silica particle. Scale bar in the inset is 50 nm. (e) Pt porous nanowire network coexisting with silica rods after partial removal of the silica. Silica rod residual is marked by a yellow arrow, nanowires are marked by a blue arrow, and a rod-shaped secondary pore is marked by a white arrow. (f) Highly porous Pt nanowire network consists of short and curved nanowires, which is prepared using the precursor solution containing 5 wt % rod-shaped colloidal silica.

arrow) are randomly oriented within the Pt nanowire network (marked by a blue arrow), which is distinct from the swirling nanowire mesostructures (Figure 1c) using spherical silica porogens. Highly porous Pt nanowire network thin films were obtained using the template synthesized from the precursor solution containing rod-shaped colloidal silica with increased amount. Figure 1f shows a low-magnification SEM image of such highly porous Pt nanowire network thin film after complete removal of both templates. The observed irregular shapes of macropores in the nanowire network are produced from the rod-shaped silica particles. Part of the macropores observed appear to be larger than the particle templates, which may result from incomplete filling of Pt within the mesopores and/or aggregation of silica rods in the precursor solution during the template formation process. TEM investigation shows the porous nanowire network is composed of a short, curved, but interconnected nanowire network (see Supporting Information, Figure S1).

From the replication process synthesizing nanowire network, it is demonstrated that 2-D hexagonal silicate/surfactant mesophases maintain their self-assembled 2-D tubular mesostructure in the presence of secondary porogens. However, 2-D tubular hexagonal domains are significantly changed. XRD investigation shows a broad (100) reflection peak and

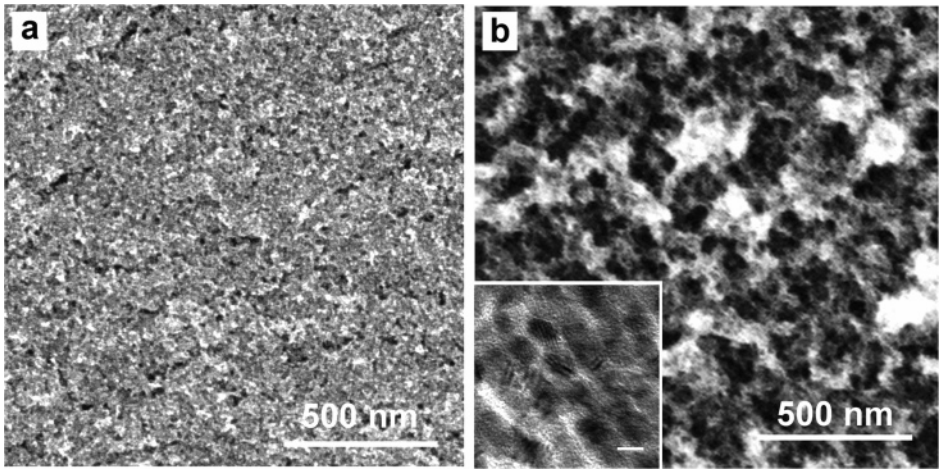

Figure 2. SEM and TEM images of Pt nanowire networks prepared using Brij-58-directed cubic-structured mesoporous silica as template. (a) SEM image of Pt mesh-like nanowire network prepared without secondary pores. (b) SEM image of a porous Pt mesh-like nanowire network prepared from cubic-structured templates containing 70−100 nm spherical silica particles as secondary porogens. (Inset) High-magnification TEM image of the Pt mesh-like nanowire network. Scale bar in the inset is 5 nm.

the absence of a (200) peak in mesoporous silica thin film doped with rod-shaped silica particles (Supporting Information, Figure S2), indicating a decreased domain size of 2-D hexagonal mesostructure. SEM investigation of the 2-D nanowire networks (Figure 1) also demonstrates that the domain size of the 2-D hexagonal mesostructure decreases with increasing concentration and size of secondary porogens in the precursor solution. Tubular mesostructure in the hexagonal domain prefers to swirl tangentially along/around colloidal silica, which also promotes formation of a more swirling defect structure in the 2-D hexagonal mesostructure.

2. Hierarchically Porous 3-D Nanowire Thin Films. In addition to controlling the hierarchical pore structure in the nanowire network using secondary porogens with different sizes and shapes, the mesostructure of the nanowire is also profoundly affected by primary mesoporous templates. Using a 3-D cubic mesoporous template instead of a 2-D tubular one, a mesh-like morphology in Pt nanowire networks is obtained (Figure 2) as compared to the wire-like morphology shown in Figure 1. The 3-D cubic structured mesoporous silica thin film is prepared using Brij-58[11] or Brij-56 surfactant. Figure 2a shows a representative top-view SEM image of a Pt mesh-like nanowire network without secondary pores, displaying a continuous, homogeneous nanowire network. It is consistent with our result reported previously.[11] Note that void spaces are also generated by aggregation of nanowires upon removal of silica templates. Figure 2b shows an SEM image of hierarchically porous Pt mesh-like nanowire network thin films prepared using Brij-58-directed cubic-structured templates containing spherical silica particles (70−100 nm). Compared with the mesh-like nanowire network shown in Figure 2a, the highly porous structure is generated due to incorporation of spherical silica particles. Macropores of 70−100 nm are clearly observed besides mesh-like nanowire domains. A high-magnification TEM image of the nanowire network is shown in the inset of Figure 2b, revealing the interconnectivity of individual nanowires with an interwire space of 1−2 nm which is similar to that of the network without secondary pores in our previous report.[11] This suggests that the presence of the secondary porogen does not alter the assembly behavior of cubic silicate/surfactant mesophases.

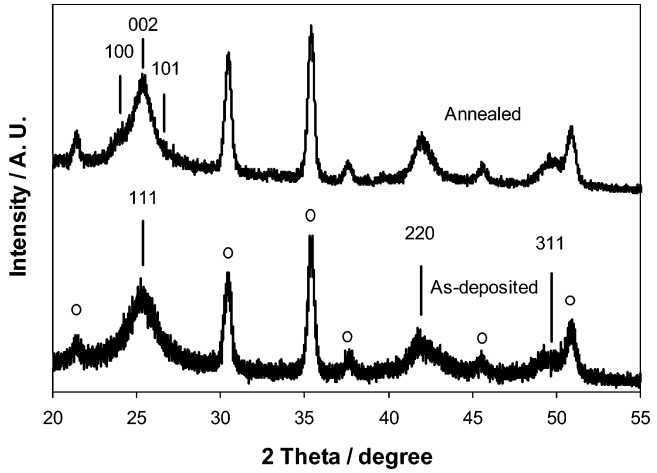

Figure 3. XRD patterns of CdSe nanowire network thin films prepared using Brij-56-directed cubic-structured mesoporous silica template. (a) As-deposited CdSe nanowire network thin film showing zinc blende structured crystalline CdSe nanowires. (b) Annealed CdSe nanowire network thin film showing slight transformation to wurtzite crystalline CdSe nanowires. The diffraction peaks of the substrate are marked by circles.

3. Hierarchically Porous CdSe Nanowire Thin Films and Photovoltaic Device. Benefitting from the capability of electrodeposition, this general synthetic approach can be extended to synthesize hierarchically porous nanowire networks with many other compositions. Here we synthesize a CdSe nanowire network with the hierarchical pore structure and demonstrate its potential to be used in fabrication of hybrid solar cells. Figure 3 shows XRD patterns of an as-deposited CdSe nanowire network thin film and an annealed sample. The as-deposited CdSe nanowire network thin film shows zinc blende cubic crystalline-structured CdSe. Due to constraint within the mesoporous silica framework, cubic crystalline CdSe nanowire networks are mostly maintained after annealing except only partial crystalline transformation to the wurtzite hexagonal structure indicated by the XRD pattern (Figure 3) and selected area electron diffraction (SAED) pattern (Supporting Information Figure S3) of the annealed sample, which is distinct from complete transfor-

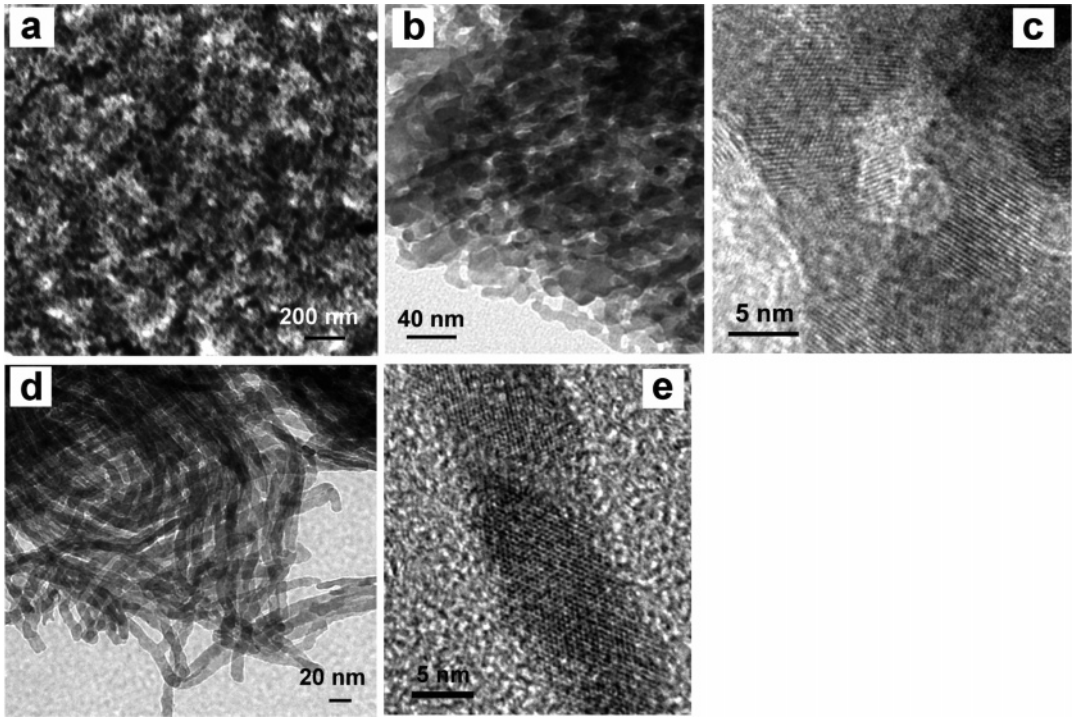

Figure 4. SEM and TEM images of annealed mesh-like CdSe nanowire networks (a−c) prepared using Brij-56-directed cubic-structured mesoporous silica templates and annealed wire-like CdSe nanowire network (d−e) prepared using P123-directed hexagonal structured mesoporous silica templates. (a) SEM image of a porous CdSe nanowire network prepared using templates containing rod-shaped secondary silica porogens. (b) TEM image of the mesh-like CdSe nanowire network. (c) High-resolution TEM image of the mesh-like CdSe nanowire network showing the crystalline lattice fringes. (d) TEM image of CdSe nanowires with average diameter of 9 nm prepared using tubular-structured mesoporous silica directed by P123. (e) High-resolution TEM image of single CdSe nanowire showing the crystalline lattice fringes.

mation to the hexagonal crystalline phase in bulk CdSe thin films.[17] The more resolved diffraction shown in the XRD and SAED pattern of the annealed sample indicates improved crystallinity of the CdSe nanowire network after annealing. Figure 4a shows an SEM image of a porous CdSe nanowire network thin film prepared using a Brij-56-directed cubic mesoporous silica template with rodlike silica particles as the secondary porogens. The reason we chose the rod-shaped porogens is that rods are likely to form an interconnected network than spherical particles. TEM investigations show that the network is composed of mesh-like CdSe nanowires (see Figure 4b). These CdSe nanowire networks are polycrystalline, and their lattice fringes are clearly revealed in the high-resolution TEM image shown in Figure 4c. Similar to the mentioned Pt, CdSe nanowire networks with wire-like morphology are also made using P123-directed mesoporous silica template. Figure 4d shows a TEM image of the CdSe nanowires with an average diameter of approximately 9 nm. The high-resolution TEM image (Figure 4e) shows lattice fringes of a polycrystalline CdSe nanowire.

Such hierarchical nanowire thin films are of interest for many device applications, such as solar cells. It has been demonstrated that hybrid solar cells can be prepared by infiltrating polythiophene within mesoporous TiO_2 thin films.[15,16,18] Such hybrid cells show higher efficiencies compared with those based on planar TiO_2 as the electron acceptor. Further improvement, however, is limited by the complete filling of polymers into mesoporous channels, the small pore size that hinders a favorable polymer chain alignment, and hole transport.[19] The present hierarchically porous semiconductor (e.g., CdSe) nanowire networks may provide an ideal platform for photovoltaic devices because of the following intrinsic advantages: (1) the nanowire networks provide a three-dimensional connectivity throughout the device thickness, facilitating charge transport, (2) the crystallinity of CdSe can be increased by annealing without aggregation, (4) the hierarchically meso/macroporous structure facilitates infiltration of hole-conducting materials into nanowire networks. The inset in Figure 5 shows the configuration of the solar cells used in this study. The CdSe nanowire networks are prepared using a Brij-56-directed cubic-structured template with rodlike silica particle as secondary porogens. Poly(3-hexylthiophene) (P3HT) were coated and annealed on top of the CdSe nanowire network to form a composite film that was sandwiched between a FTO-coated glass slide and an evaporated Au electrode. Figure 5a shows a $I-V$ curve of the solar cell device using a CdSe nanowire network without any secondary pores, characteristic of an effective diode from dark field. The

(14) Huynh Wendy, U.; Dittmer Janke, J.; Alivisatos, A. P. Hybrid nanorod-polymer solar cells. *Science* **2002**, *295* (5564), 2425−7.
(15) Wang, H.; Oey, C. C.; Djurisic, A. B.; Xie, M. H.; Leung, Y. H.; Man, K. K. Y.; Chan, W. K.; Pandey, A.; Nunzi, J. M.; Chui, P. C. Titania bicontinuous network structures for solar cell applications. *Appl. Phys. Lett.* **2005**, *87* (2).
(16) Coakley, K. M.; McGehee, M. D. Photovoltaic cells made from conjugated polymers infiltrated into mesoporous titania. *Appl. Phys. Lett.* **2003**, *83* (16), 3380−3382.
(17) Gorer, S.; Hodes, G.; Sorek, Y.; Reisfeld, R. Crystal phase transformation in sol−gel films of nanocrystalline CdSe and CdS. *Mater. Lett.* **1997**, *31* (3−6), 209−214.
(18) Bartholomew, G. P.; Heeger, A. J. Infiltration of regioregular poly-[2,2′-(3-hexylthiopene)] into random nanocrystalline TiO2 networks. *Adv. Funct. Mater.* **2005**, *15* (4), 677−682.
(19) Coakley, K. M.; McGehee, M. D. Conjugated Polymer Photovoltaic Cells. *Chem. Mater.* **2004**, *16* (23), 4533−4542.

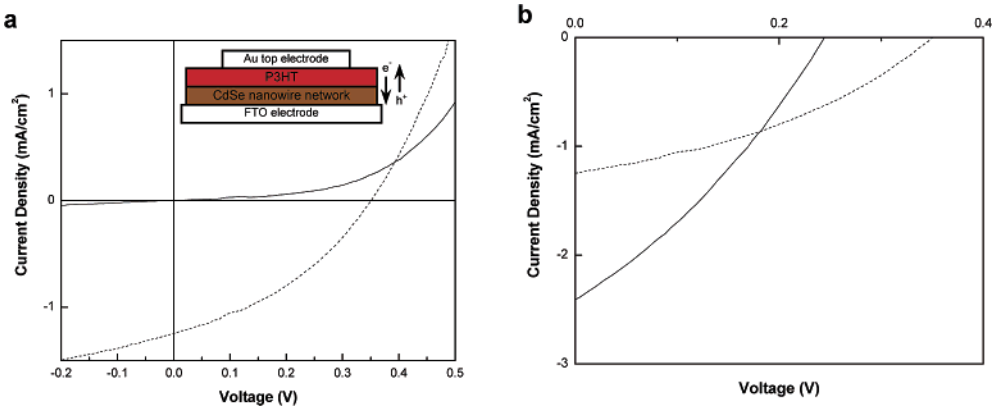

Figure 5. Performance of FTO/CdSe nanowire network/P3HT/Au photovoltaic cells. (a) $I-V$ response of a photovoltaic cell using CdSe nanowire network without any secondary pore structure in the dark (solid line) and under simulated sunlight illumination of 100 mW/cm^2 (dashed line). (Inset) Device structure of the FTO/CdSe nanowire network/P3HT/Au photovoltaic cell. (b) $I-V$ curves of solar cells fabricated using CdSe nanowire network with (solid line) or without (dashed line) secondary pore structure under simulated sunlight illumination of 100 mW/cm^2.

photovoltaic device yields an open-circuit voltage (V_{oc}) of 0.35 V, a short-circuit current density (J_{sc}) of 1.25 mA/cm^2, a fill factor of 0.37, and a power efficiency of 0.16% under simulated sunlight with an intensity of 100 mW/cm^2. CdSe nanowire networks with secondary pores are also examined in the solar cell to illustrate the positive effect of having macropores in the nanowire network matrix. Figure 5b compares the light $I-V$ curves of the hybrid solar cells prepared using CdSe nanowire networks with/without secondary pore structure. The photovoltaic device using a porous CdSe nanowire network yields an open-circuit voltage (V_{oc}) of 0.25 V, a short-circuit current density (J_{sc}) of 2.4 mA/cm^2, a fill factor of 0.3, and a power efficiency of 0.18% under simulated sunlight with an intensity of 100 mW/cm^2.

As the primary pore size of the nanowire network is 2−3 nm, we believe most of the polymer is on top of the surface of the CdSe nanowire networks. The interface of the CdSe nanowire network/polymer heterojunction is thus planar in the absence of secondary pores. Hierarchical porous CdSe nanowire network thin films show a porous, rough surface which may lead to increased interfacial area between the CdSe nanowire networks and the P3HT in the hybrid solar cell. A photocurrent increase using the porous CdSe nanowire network as an electron acceptor mainly attributes to such a porous and rough heterojunction interface after introduction of secondary pore structure into CdSe nanowire networks. Current photovoltaic values are still limited by our device structure, and more appropriate electrode materials have to be chosen.[20,21] Further device optimization, such as pore organization, polymer thickness, top electrode choice, and modification of interface between CdSe and polymer, may improve the efficiency of the solar cell, which is beyond the scope of our focus in this work. Nevertheless, the performance of the photovoltaic devices demonstrates the possibility of using CdSe nanowire networks as an electron acceptor in solar cells and confirms the roles of hierarchical pore structure in device applications.

Conclusion

In summary, we demonstrated a ready and efficient route to fabricate hierarchical, continuous, porous nanowire network thin films. This novel approach provides various nanowire network thin films with tunable pore structure (e.g., isolated and interpenetrated), pore shape (e.g., rodlike or sphere), and composition (e.g., metal and semiconductor). CdSe nanowire network thin films have been demonstrated as electron acceptors in the fabrication of a CdSe nanowire network/poly(3-hexylthiophene) hybrid solar cell. The hierarchically porous structure facilitates infiltration of the polymer in the CdSe nanowire network, resulting in a photovoltaic with significantly increased photocurrent which may be attributed to the increased junction areas formed. The novel nanowire network with controllable pore structure will open up new applications in energy storage such as photovoltaic, capacitor, thermoelectric, etc.

Acknowledgment. The authors gratefully acknowledge the support of this work by Office of Naval Research, National Science Foundation (CAREER Award and NER-CTS) and Louisiana Board of Regents.

Supporting Information Available: Three additional figures. This material is available free of charge via the Internet at http://pubs.acs.org.

CM052216B

(20) Huynh, W. U.; Dittmer, J. J.; Teclemariam, N.; Milliron, D. J.; Alivisatos, A. P.; Barnham, K. W. J. Charge transport in hybrid nanorod-polymer composite photovoltaic cells. *Phys. Rev. B: Condens. Matter Mater. Phys.* **2003**, *67* (11), 115326/1−115326/12.

(21) Arango, A. C.; Johnson, L. R.; Bliznyuk, V. N.; Schlesinger, Z.; Carter, S. A.; Horhold, H.-H. Efficient titanium oxide/conjugated polymer photovoltaics for solar energy conversion. *Adv. Mater.* **2000**, *12* (22), 1689−1692.